

A Study of Three Finite-Difference Schemes and Their Role in Asynoptic Meteorological Data Assimilation

ISIDORE HALBERSTAM¹

Institute for Space Studies, Goddard Space Flight Center, NASA, New York, N. Y.

(Manuscript received 23 January 1974, in revised form 2 May 1974)

ABSTRACT

An investigation of three finite-difference methods and their response to the insertion of simulated satellite data is presented. A simple one-level barotropic model is used as the "forecast" model, while the Mintz-Arakawa two-layer model is used to furnish the initial field, the verification fields, and the simulated satellite data. The schemes tested are the Shuman, the Matsuno-TASU, and an implicit scheme devised by McPherson. Results indicate that the schemes react to inserted data as they would react to unfiltered initial fields. The schemes which contain significant implicit viscosity are capable of damping the high-frequency oscillations which occur after insertions, but such schemes may cause a loss of information. The schemes which contain less damping capability produce "shock" waves which damage the forecasts. It is also found that insertion of winds along with temperature data improves the forecast considerably.

1. Introduction

The use of asynoptic satellite data to update integrations of numerical atmospheric circulation models has been the subject of much numerical experimentation recently. Most experiments deal with what has come to be known as four-dimensional data assimilation, which consists of the insertion of data directly into the model at the appropriate grid point and time step of the calculation. The data are usually atmospheric temperature profiles derived from infrared radiance measurements. It is hoped that by replacing enough computed temperature values with actual temperature measurements, the other field variables will adjust themselves to the observed temperature profiles, and the forecast values will approach reality. Simulation experiments have been performed using computer-produced temperature fields. One major obstacle to the direct insertion of data, discovered during these experiments as well as during experiments involving actual satellite soundings, is the production by the model of small computational waves after the insertion, because of the sudden gradient imposed by the insertion. If the inserted temperature data are significantly out of balance with the velocity field, large-scale gravity oscillations may occur. Both the computational and physical waves have commonly been referred to as "shock" waves because of parallels in the creation of these waves and the shock waves in classical aerodynamics. These shock waves may eventually dissipate, but they may leave in their wake a fore-

cast which hardly shows the effect of the insertion. In a recent experiment, Jastrow and Halem (1973) have discovered that when actual data are inserted, as opposed to model-generated data, the shock effect is more noticeable probably because the model is more attuned to data which it has produced. The other field variables therefore adjust better in the simulated experiments approaching a lower level of error than with real data.

Various means to control these shocks were discussed in the 1971 Symposium on Four-Dimensional Analysis at Princeton. Some workers believed that a weighting of data before insertion would reduce the shocks while still accomplishing the same goal of updating the forecast field. Others argued that insertions of data with or without weights would accomplish the same results. [Kasahara (1972) gives a brief review of most papers presented at the symposium.] Recently, Hayden (1973) has shown that by means of "dynamic balancing," the effect of insertions can be enhanced. Dynamic balancing was conceived in an effort to deal with the problems of initializing the field of variables for numerical models. It consists of adjusting the wind, temperature and pressure fields so that they are in dynamic balance and do not give rise to false waves which may disrupt the forecast. The insertion of data is similar in many ways to the initialization of the field and can thus be treated in a similar fashion. Thus, a localized dynamic balancing of the area about an insertion should improve the updating process.

Experiments and discussions dealing with four-dimensional analysis usually contain little mention of

¹ Current affiliation: Jet Propulsion Laboratory, California Institute of Technology, Pasadena.

the models and their respective differencing schemes. Although many experiments have been performed at different research centers using different models, there is a need to investigate the effect of the models themselves, especially with respect to their characteristic differencing schemes, on conclusions concerning insertions. This study is an attempt to demonstrate the response of various finite-difference schemes to the insertion of unweighted data. Using a simple barotropic model as a forecast model and the Mintz-Arakawa (M-A) two-level general circulation model as a source of data, three schemes will be tested in regard to their ability to assimilate inserted data effectively. These schemes are: 1) a Shuman scheme employing centered time differences and 9-point spatial smoothing; 2) a Matsuno-TASU scheme, which uses a predictor-corrector time differencing and an alternating, staggered space differencing; and 3) a semi-implicit scheme similar to one proposed by McPherson (1971) using much larger time steps than allowable with the first two schemes.

2. Design of the experiments

The model used to test the response of the differencing schemes was a one-level barotropic model containing three equations relating velocity and geopotential height. Data selected for initial conditions, boundary conditions, insertion data, and verification data were obtained from the two-layer M-A model described by Gates *et al.* (1971). All the data were from a computer-simulated February situation. Forecasts were made up to 24 hr at the 500-mb level and verified against the M-A fields at 6-hr intervals. The domain for all forecasts was limited to an area slightly larger than the North Pacific Ocean, extending from approximately 2 to 70N and running westward from 110W to 130E. The restricted domain necessitated some specification along the four boundaries. This was accomplished by inserting M-A data at the boundary points at each time step, thereby preventing boundary effects from ultimately ruining the forecasts. The grid system employed was entirely similar to the M-A staggered grid system in order to avoid interpolation procedures, although this unrealistically tuned the forecasting model to the inserted data. The grid increment in the east-west direction, Δx , is 5° longitude, while the north-south unit increment, Δy , is 4° latitude.² The grid is staggered in the sense that not all variables are calculated at the same grid points. In the M-A model, the thermodynamic variables are calculated on grid points separate from the points at which wind velocities or mass transport terms are calculated. The barotropic model has only three vari-

ables, but its grid is also staggered, with geopotential heights calculated on one grid and the components of wind velocity calculated on a grid staggered $2\frac{1}{2}^\circ$ west and 2° south of the height grid.

The equations for the barotropic model are similar to the equations governing the free surface conditions of a shallow fluid. The equations contain no sources or sinks of energy except at the boundaries, but divergence of the velocity fields does exist, and hence vorticity is not conserved. The equations are

$$\left. \begin{aligned} \frac{\partial u}{\partial t} + mu \frac{\partial u}{\partial x} + v \frac{\partial u}{\partial y} - fv + m \frac{\partial \phi}{\partial x} &= 0 \\ \frac{\partial v}{\partial t} + mu \frac{\partial v}{\partial x} + v \frac{\partial v}{\partial y} + fu + \frac{\partial \phi}{\partial y} &= 0 \\ \frac{\partial \phi}{\partial t} + mu \frac{\partial \phi}{\partial x} + v \frac{\partial \phi}{\partial y} + \phi \left(m \frac{\partial u}{\partial x} + \frac{\partial v}{\partial y} \right) - m^{-1} \phi v \frac{\partial m}{\partial y} &= 0 \end{aligned} \right\} \quad (1)$$

where u is the westerly wind component, v the southerly wind component, ϕ the geopotential, f the Coriolis parameter, and m the map factor (in this case nothing more than the secant of latitude). The independent variables are the east-west distance x , the north-south distance y , and the time t .

The experiments used the barotropic model as a forecast model, while the M-A model was regarded as the ideal state or "nature." By inserting data from the M-A model into various numerical approximations to (1) and measuring the degree to which the forecast was improved by the insertion, some conclusions could be formed regarding the effect of particular numerical schemes on the updating process. These insertions were performed at each time step, along paths representing the swaths of satellite observations, by merely replacing the calculated values found at all grid points within the swath with data from the M-A model. The entire domain was covered by the equivalent of three staggered satellite passes in approximately 4–5 hr of simulated time, and all grid points had their values replaced once and only once in that period. The width of each of the three swaths is ~ 800 km, implying a side scan capability of 400 km from the sub-satellite point. The inserted data were assumed ideal in that no "error" was added to the M-A data, nor were any grid points "unobservable."

For each numerical scheme tested, the experimental procedure was as follows:

- 1) A 24-hr control forecast was made using the prescribed initial field. The rms differences between the forecast and the M-A fields were calculated at 4, 5, 6, 12, 18 and 24 hr. The spectrum of kinetic energy over the central latitude (39N) was determined at each hour and averaged over 12 hr.

- 2) Using the same initial conditions, a second 24-hr integration was made with M-A data inserted at each

² The time increment Δt was 6 min for both the M-A model and the barotropic model, when both the Shuman and Matsuno-TASU scheme were applied; the semi-implicit scheme allowed for a 30-min time increment.

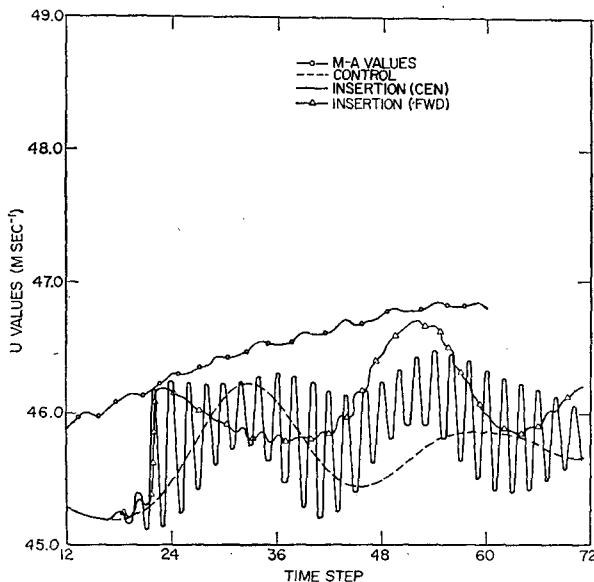


FIG. 1a. Time change of u (m sec^{-1}) at the central grid point using the Shuman scheme, for the control run, the insertion run maintaining centered differences (CEN), the insertion run with forward differences at the time and point of insertion (FWD), and the M-A data to 6 hr. The time step is 6 min.

time step until all grid points were covered once. This means that insertions were only performed for the first 4–5 hr, while the model continued to forecast until 24 hr. The data consisted of all three variables (u , v , ϕ) except in one instance which will be explained below. The rms differences and energy spectrum were calculated for the insertion case as well.

3) Another forecast was made differing from the control only in that the initial conditions were perturbed by random errors. These errors were uniformly distributed with mean zero. The rms differences between the perturbed initial field and the non-perturbed initial field were 3.19 m sec^{-1} for u , 1.02 m sec^{-1} for v , and 32.46 gpm for ϕg^{-1} , where g is the gravitational constant, 9.80 m sec^{-2} . This forecast was made without any insertions.

4) Starting with the perturbed initial conditions, another 24-hr run was made with insertions to update the integration.

The rms errors did not asymptote by 24 hr, nor were they expected to do so. Yet integrations were not carried out for longer periods because the purpose here was to investigate the effect of insertions on short-term forecasts rather than possible initialization through long-term insertions of both synoptic and asynoptic data. In fact, the 24-hr forecast can be regarded as a 19–20 hr forecast based on an initial field derived after 4–5 hr of insertion.

This 4-step procedure was followed for each of the three schemes tested. In steps 2 and 4, however, varying methods of insertion were tested. The details

and results of these experiments will be discussed in the ensuing sections.

3. Results of the experiments

a. The Shuman scheme

The first scheme investigated is one which is in operation in various models, notably at the National Meteorological Center in Washington, D. C. Details of this scheme, named after F. Shuman, are outlined by Haltiner (1971). Briefly, the scheme uses the eight points contiguous to a central grid point in taking differences (see Appendix). This results in significant spatial smoothing at each time step. The time differencing is generally centered except that some time smoothing is usually required to avoid the separation of the solution during even and odd time steps. Because of the relatively short forecast period involved in this experiment, no time smoothing was introduced except as applied to the insertions as will be fully explained below. The implicit viscosity of the Shuman scheme is quite small compared with many other schemes, so that small waves can grow considerably (see, for example, Grammelvedt, 1969). It is therefore advisable to adjust the initial wind field by the use of the balance equation or by eliminating the non-divergent component of the winds and substituting the divergent component of the forecast wind field.

Similar sensitivity was encountered when data were inserted during the experiments. In addition to small oscillations arising due to physical waves, computational difficulties were encountered because of the centered time differencing. The insertion of raw data at any grid point initiated a computational oscillation due to the alternating effect of the centered time differencing. This latter defect was remedied by “re-initializing” the point of insertion; that is, by employing a forward time step at the point of insertion and at the time of insertion, similar to the forward difference employed over the entire field at the initial time step. This simple procedure eliminated the destructive computational mode and reduced the error in prediction considerably. Fig. 1a shows the change in time of u at the central grid point for the control forecast, the M-A data, the forecast with insertions without adjusting the centered differencing (CEN), and the forecast with insertions but with forward differencing applied at the point of insertion (FWD). The insertion takes place for this particular grid point at time step 22 and its effect on the velocity values is depicted until time step 72, long enough for a definite wave pattern to appear. No M-A data, however, were available beyond 6 hr (time step 60). The CEN and FWD forecasts differ significantly afterward. The CEN curve indicates a high-frequency oscillating wave, while the FWD forecast shows no such tendency. The wavelength of the FWD forecast curve seems to be equal to the wavelength of the control forecast

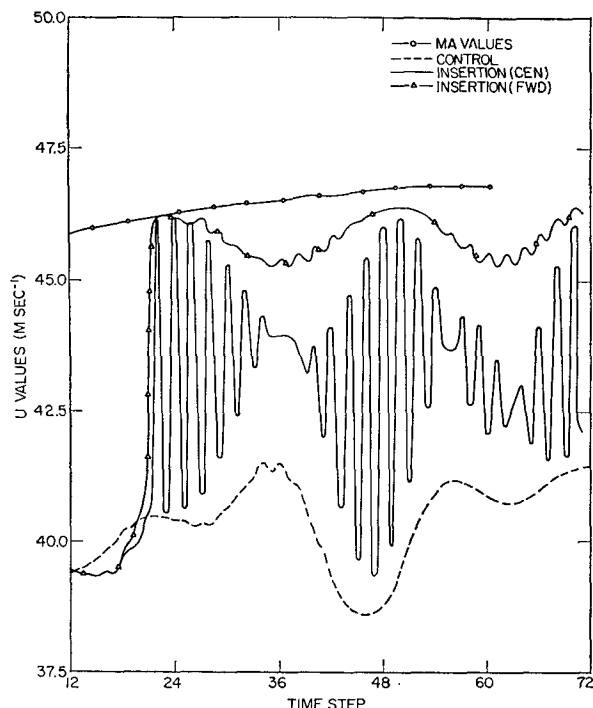


FIG. 1b. As in Fig. 1a except that random errors are present in the initial conditions.

curve, although it is notably out of phase with the control and is closer to the M-A data. The effect of the forward differencing is to have the model "forget" the prior calculated data and begin the computation from an almost new initial state. This effect is even more noteworthy when there are random errors present in the initial data. In this case, the forward differencing helps cancel not only the effect of the divergence of the forecast from the M-A model but also the effect of the initial random error, as can easily be observed in Fig. 1b. The CEN forecast, on the other hand, oscillates with even greater amplitude than in the former case because of these two effects.

The growth of rms errors when initial conditions were unperturbed showed the same pattern for all three schemes. They all exhibited monotonic increases of rms errors for the first few hours, but with the rate of growth much smaller when insertions were performed. Results of the experiments involving perfect initial conditions are omitted in favor of the more interesting experiments involving perturbed initial conditions. Fig. 2 demonstrates the impact of the insertions on rms error growth. Starting with initial random errors, there is a period of adjustment where there is no significant increase of rms error even for the control forecast. (This adjustment may be related to the filtering of high wavenumbers present in the initial field which are present neither in the forecasts nor in the verification field from the M-A model. In the real world, however, the high wavenumbers

are present in the verification fields as well and this adjustment period will probably not exist.) During this time, the insertions help reduce the rms errors to levels lower than their initial state. The FWD forecast is decidedly more efficient in reducing the error level, so that by 5 hr, the error level reached is the same as the level of error produced by the FWD forecast starting from perfect initial conditions (not shown). In other words, the FWD forecast effectively "forgets" the poor initial conditions and bases its predictions on the updated inserted data.

b. The Matsuno-TASU scheme

The numerical scheme of the M-A model is one which is temporally a predictor-corrector scheme while spatially it uses a time-alternating space-uncentered (TASU) scheme (see Appendix). Arakawa (1972) demonstrates the merit of this scheme in a simple example involving the two-dimensional shallow-water equations without dissipation terms, but with a point source and point sink present in the region. All other schemes tested showed a false alternating pattern instead of a monotonic decrease of the height toward the sink. The Matsuno-TASU scheme, however, produced results which were realistic with a decrease in height from every direction toward the sink. The scheme's

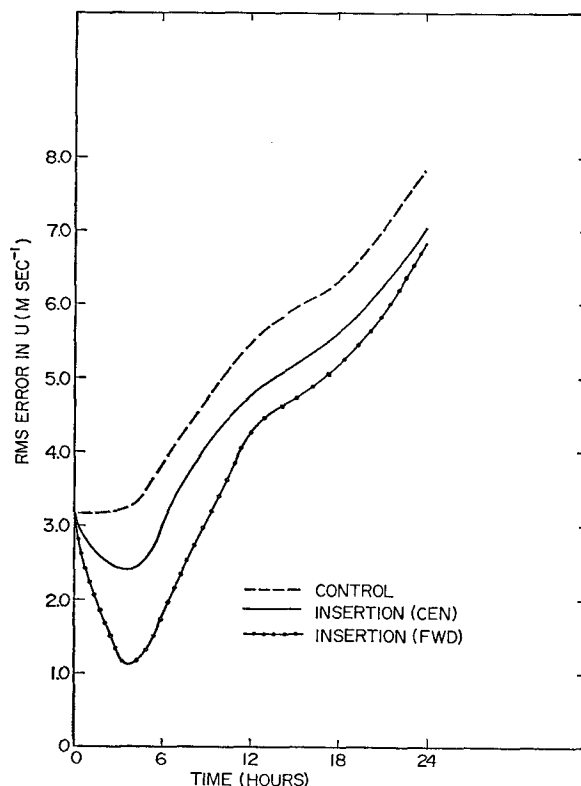


FIG. 2. Growth of rms error in u ($m\ sec^{-1}$) for the Shuman scheme for the control case, insertions with CEN, and insertions with FWD. Random errors were present in the initial conditions.

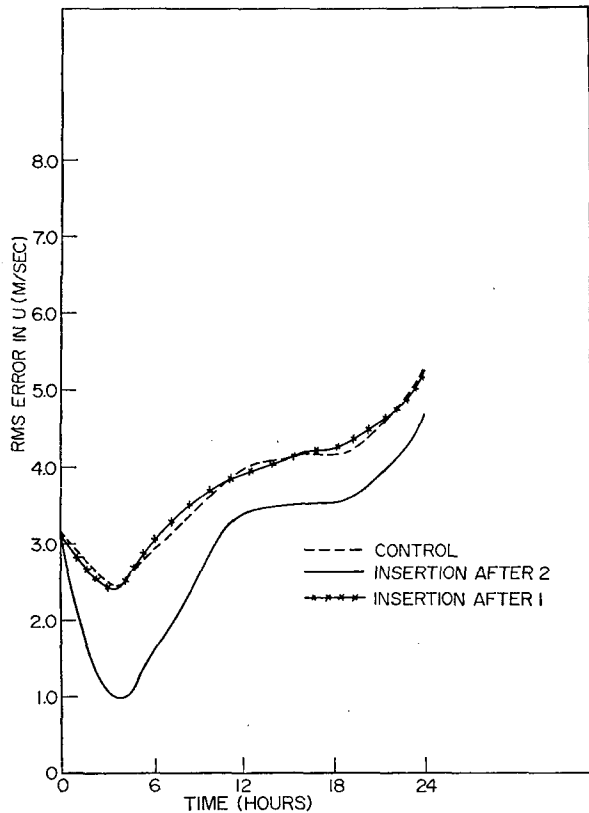


FIG. 3. Growth of rms error in u for the Matsuno-TASU scheme for the control case, insertions after the first half time step (after 1), and insertions after the full time step (after 2). Random errors were present in the initial conditions.

effectiveness is due to the combination of the two-step Matsuno scheme and the alternating space differencing of the TASU scheme.

The Matsuno scheme involves predicting an intermediate value of the variable being dealt with, then using that value to arrive at the desired forecast. That is, if Q is the variable to be predicted at time step $n+1$, given Q at time n , then a quantity Q^* is determined so that

$$Q^* = Q^n + f(Q^n), \quad (2)$$

where the superscript refers to the time level and $f(Q)$ is the algorithm involving known values by which the prediction is made. The quantity Q^* is now substituted for Q^n in the algorithm to obtain

$$Q^{n+1} = Q^n + f(Q^*). \quad (3)$$

The Matsuno scheme, although comparatively costly in computer time, can filter some of the small waves efficiently, because of its implicit viscosity. This viscosity, after insertions are made, may diminish their beneficial effect while damping the shocks. This aspect will be discussed more fully below.

The TASU scheme involves shifting the space differences to alternately the upper-right then the lower-

left portion of the grid box surrounding any point. In the experiment here and in the M-A model the TASU step is invoked only once every five time steps and then only during the second half of the time step. At all other times, the space differencing is centered.

In the experiments involving the Matsuno-TASU scheme, insertions of two kinds were made. Since the Matsuno time steps consists actually of two half-steps, i.e., one predictor and one corrector, it is possible to insert values after either half of the time step. That is to say, it is possible to substitute at a particular grid point at some given time an observed value of Q for either Q^* or Q^{n+1} [where Q , Q^* and Q^{n+1} have the same meaning as in (2) and (3)]. Upon attempting both forms of insertion, it was found that inserting after the first half step given by (2) [herein referred to as "insertion after 1"] was far inferior to inserting after the second half given by (3) [herein referred to as "insertion after 2"]. This was probably due to the strong damping effect the second half-step had on the inserted data, their influence being greatly reduced and the forecast barely, if at all, improved because of the insertion.

Fig. 3 demonstrates the effect of the insertions on the rms error for the experiment where initial error was present. Only insertion after 2 results in a meaningful reduction of rms error; insertion after 1 is almost indistinguishable from the control case. All cases resulted in an initial adjustment period during which the rms error was substantially reduced. When insertions took place during the first few time steps, the rms errors were reduced to values significantly lower than the rms errors of the control forecast.

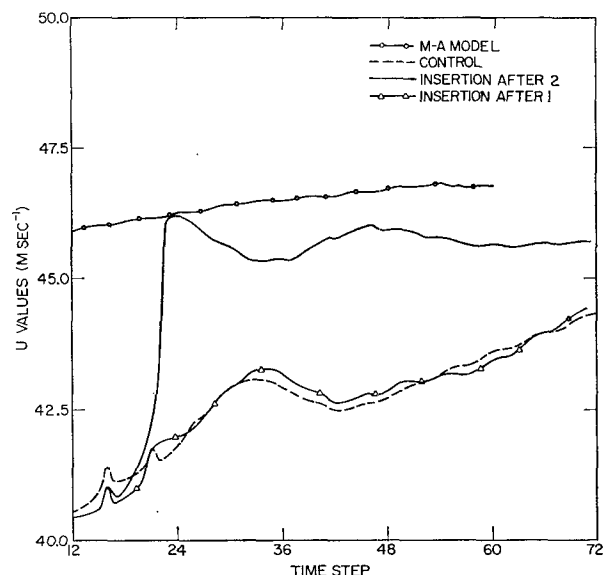


FIG. 4. Time history of u at the central grid point during Matsuno-TASU experiments for the control case, insertion after 1, insertion after 2, and the M-A data to 6 hr. Random errors were present in the initial conditions. The time step is 6 min.

The appearance of this adjustment period and its obvious reinforcement by the insertions may possibly be explained as the result of filtering by both the barotropic and the M-A models. By perturbing the initial conditions with random error, small waves are probably produced. The M-A model successfully filters these waves, so that the verification fields and the satellite data are devoid of these high wavenumbers. The barotropic model because of its spatial resolution and with the assistance of the Matsuno-TASU scheme begins filtering these waves as well, making its early forecasts more compatible with the M-A fields despite the predictability factor. If M-A data are inserted, the filtering is apparently accelerated and the rms error reduced finally to a level which is nearly independent of the initial state. Whether this will occur if actual atmospheric data are used is doubtful, but can only be verified through actual experiment.

Fig. 4 displays the time history of u at the central point of the grid network. It demonstrates clearly the effectiveness of the insertion on updating the model. The control case and insertion after 1 result in values which are substantially different from the M-A data. When insertion after 2 takes place, however, the value of u is rapidly brought closer to the M-A data and stays there for some time. None of the severe oscillations produced by the Shuman scheme are present in this experiment, indicating once again the strong damping of the Matsuno-TASU scheme.

c. The semi-implicit scheme

Implicit and semi-implicit schemes are often more economical than explicit schemes subject to the Courant-Friedrichs-Lewy condition for linear stability. By expressing more than one term at the forecast $(n+1)$ time level, larger time increments are possible without causing instabilities. The larger time steps, however, imply that longer periods can be considered synoptic with respect to the insertion of data. Satellite data which are gathered over the entire period of the time increment Δt are inserted at one instant. What effect this wholesale insertion has on the updating process depends on many factors, among them the nature of the data themselves and their change with time.

The experiment conducted involved a scheme recently developed by McPherson (1971). This scheme separates the advective terms from the other terms of the equation which are evaluated at the forecast time (see Appendix for details). By cross differentiation the velocities can be eliminated, leaving a Helmholtz equation of the form

$$\nabla^2 \phi^{n+1} - \lambda \phi^{n+1} (D^2 \phi^n)^{-1} = \lambda F_{i,j} (D^2 \phi^n)^{-1}, \quad (4)$$

where

$$D = \begin{cases} \Delta t, & n=1 \\ 2\Delta t, & n \neq 1 \end{cases}, \quad \lambda = 1 + f^2 D^2,$$

and F is some known function of space at any given time step; ∇^2 is a numerical approximation to the Laplacian operator ∇^2 . The superscript represents the time step at which the variable is being evaluated. Once ϕ^{n+1} is evaluated from (4), it is a simple matter to determine u^{n+1} and v^{n+1} . Eq. (4) is solved by using a relaxation technique, starting from some initial guess of ϕ^{n+1} . For this set of experiments, a time increment of $\frac{1}{2}$ hr was selected, which reduced computation time to about one-half of that required for the Matsuno-TASU scheme despite the iterations required for the relaxation.

In addition to the insertion experiment involving the assimilation of data from all variables at each time step, an attempt was made here to measure the efficacy of inserting geopotential heights alone. This is similar to the practice of inserting only temperature lapse rates which are derived from infrared radiance measurements. When contrasted with results obtained from the insertion of all variables, the experiment could indicate whether the "balancing" of the velocity fields is substantially beneficial to the assimilation process given the grid size and the data characteristics for the experiment. When perfect initial conditions are used, the insertion of all variables does not create a significant improvement over the insertion of the temperature field alone. There is, expectedly, a lower level of error when all variables are inserted simply because the quantity of inserted data is greater. When random error is added to the initial conditions, however, the dynamic balancing accomplished by the insertion of wind data along with the heights produces significant improvements in the forecast. Fig. 5 shows the rms error growth for u when random errors are present in the initial state. As in the case of the Matsuno-TASU scheme, the first few time steps result in an adjustment which lowers the rms error even if no insertions are performed. The degree of adjustment is limited when only heights are inserted, but a significant dip occurs when all variables are inserted. The level of rms error reached through insertion at 5 hr is again equivalent to the level reached when inserting after perfect initial conditions (not shown), indicating that the insertions update the computations efficiently despite the larger time increment of the semi-implicit scheme.

Fig. 6 depicts the time change of the variable u at the central grid point for the various experiments with the semi-implicit scheme. Because of the larger time increment, only 15 time steps are presented, so that the simulated time lapse is consistent with earlier figures. Despite the random errors present in the initial conditions, the control run does not give rise to oscillations. When ϕ alone is inserted, the change in u values is not significant for at least 15 time steps. The insertion of all variables does, however, have a notable effect which gives rise to oscillations similar to,

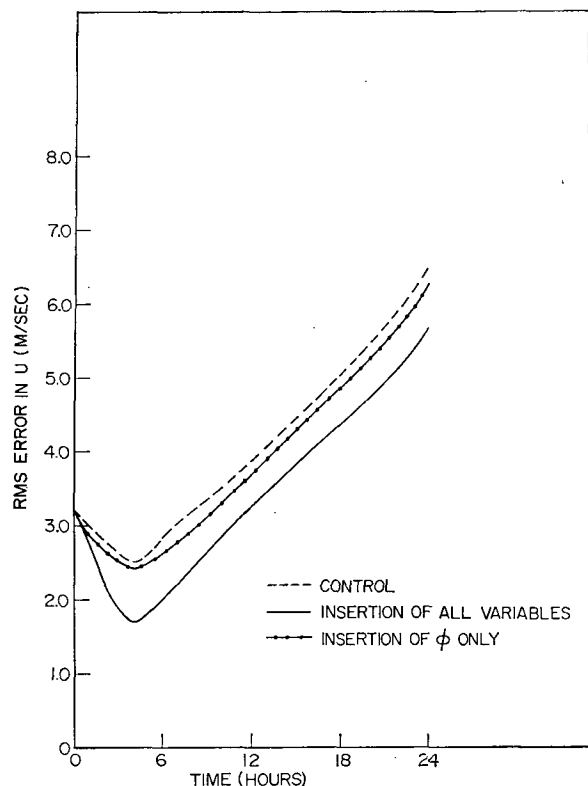


FIG. 5. Growth of rms error in u for semi-implicit scheme for the control case, insertion of all variables (u, v, ϕ), and insertion of ϕ alone. Random errors were present in the initial conditions.

but not quite as large as, those produced by the Shuman scheme. The large time steps are perhaps a factor in creating these oscillations. Large doses of data are injected at each time step and only limited filtering can be performed because of the few steps that follow the insertion. It may prove beneficial to reduce the time step immediately following insertion so that the adjustment to the model may take place in a relatively short period of simulated time.

4. Energetics and comparisons

A study of the energetics involved in the various numerical schemes was performed by calculating the kinetic energy over the central latitude as a function of zonal wavenumber. The wavenumbers mentioned here are not global but refer to the domain of integration. Only one-third of the Northern Hemisphere is represented on this domain, so that wavenumbers should be multiplied by 3 in order to correspond to full-latitude wavenumbers. The kinetic energy was calculated at each hour and averaged over 12 hr. Only one latitude was involved; too much spatial averaging may have resulted in disguising the effect of the insertions.

When perfect initial conditions were used, few departures from the control energy spectrum were

observed after insertions. When random errors were present initially, however, the insertions managed to return the spectra to the non-perturbed control spectra. The effect of the random errors was to shift energy from low wavenumbers to higher ones probably because of the creation of small wave disturbances. The insertion of data from the M-A model counteracted this trend and shifted the energy back to the unperturbed spectral distribution. Fig. 7 shows the various spectral distributions with and without insertions. For all three numerical schemes, the optimum method of insertion (from an rms standpoint) is seen to increase kinetic energy in the region of wavenumbers 1 and 2. Between wavenumbers 2 and 4 there is a crossover, and kinetic energy is lower for the insertion experiments for these higher wave numbers. Wave 5 is anomalous in all three experiments, a local minimum being achieved by the control but not by the insertion spectra. Beyond wave 5, there are variations among the three schemes, but this is to be expected in the sensitive low energy regions.

The three schemes also demonstrated varying degrees of skill in forecasting. The Matsuno-TASU scheme reached lower levels of rms error than either of the two other schemes. The Shuman scheme, although greatly enhanced by the insertions, has a large error growth rate. The semi-implicit scheme produces rms errors at 24 hr which lie between those produced by the other two. No generalizations should be drawn from this behavior, however, as to the forecasting ability of a particular scheme. It must be remembered that the data for verification were derived from the

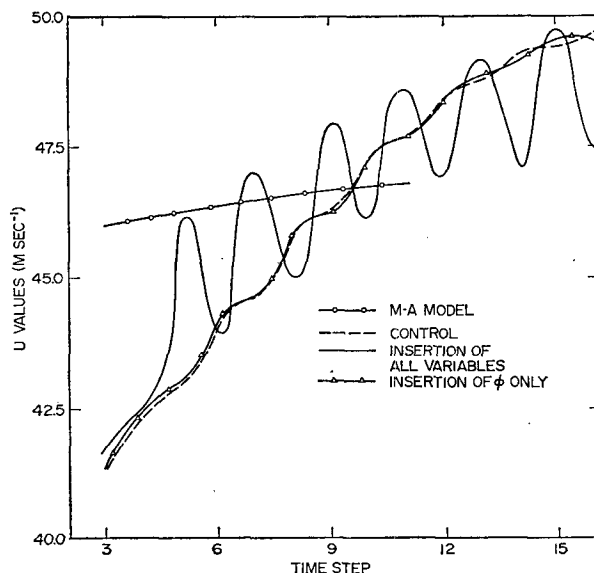


FIG. 6. Time history of u at the central grid point during semi-implicit scheme experiments including the control, insertion of all variables, insertion of ϕ only, and the M-A data to 6 hr. Random errors were present in the initial conditions. The time step is 30 min.

M-A model, which itself uses a Matsuno-TASU differencing scheme, and not from observations of the real atmosphere. All that can be properly assumed is that data produced by the barotropic model using the Shuman scheme do not correlate well with data produced by the M-A model using the Matsuno-TASU scheme. A better test of this would be to use the same model, but with different finite-difference schemes, to produce forecasts which could then be examined and compared.

5. Conclusions

Three numerical schemes have been examined with respect to their reaction to the sequential insertion

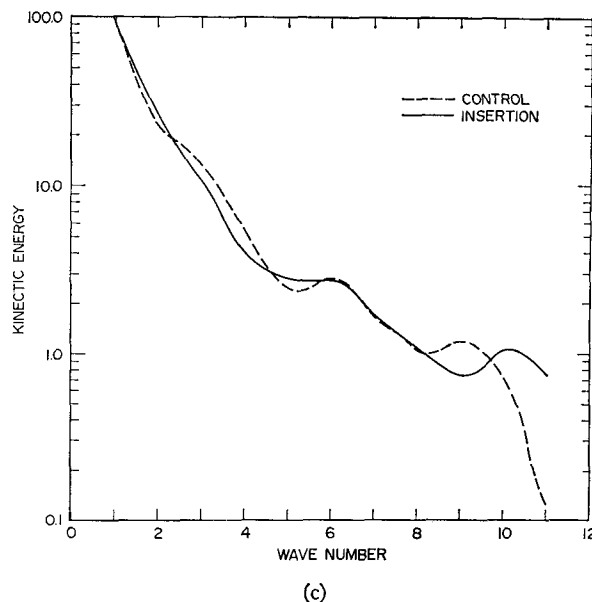
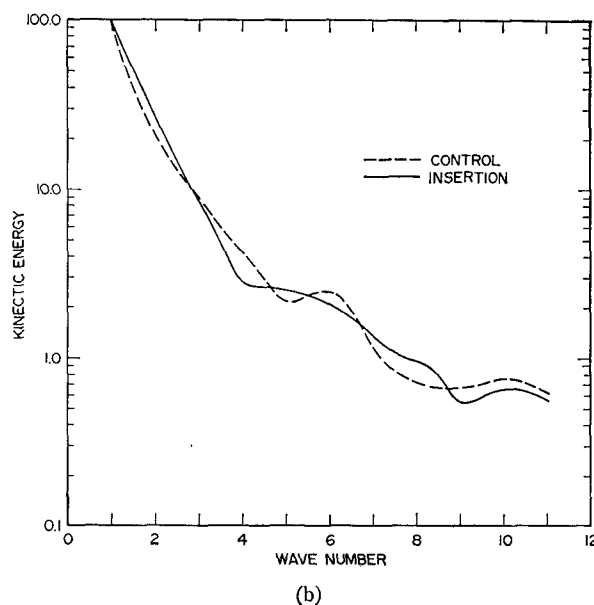
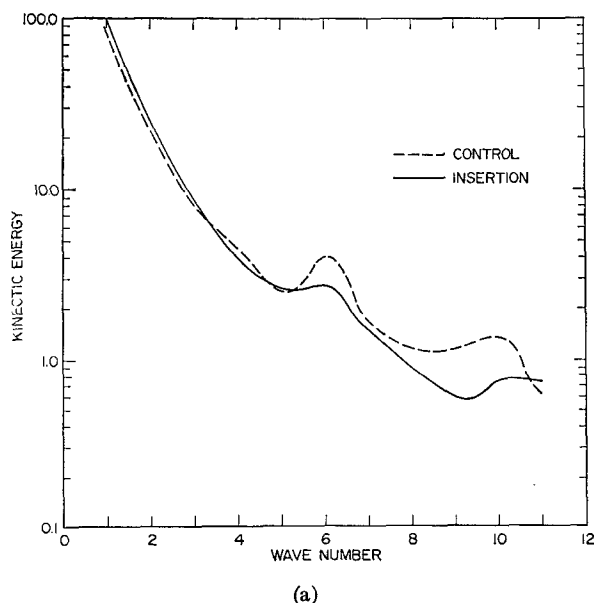


FIG. 7. Kinetic energy ($\text{m}^2 \text{sec}^{-2}$) spectra averaged over 12 hr for the central latitude (39°N) for the control case and the most effective insertion of (a) the Shuman scheme, (b) the Matsuno-TASU scheme, and (c) the semi-implicit scheme.

of data into various grid points during computation. Comparisons were made on the basis of rms errors, the time history at an individual grid point, and the 12-hr spectra of kinetic energy.

Results indicate that inserting can be an effective means of updating model integrations regardless of the numerical scheme, but that some care must be taken as to how the insertions are to be performed. The Shuman scheme proved very sensitive to the inserted data, and severe oscillations could result if centered time differencing is retained during the insertion process. The Matsuno-TASU scheme, on the other hand, proved capable of filtering spurious short waves effectively, but insertions had to be made after the complete time step or the influence of the data might be lost. The semi-implicit scheme gave rise to some oscillations despite its damping mechanism, probably due to the larger dose of data inserted at each time step and the smaller number of time steps needed to achieve a forecast. In general, the schemes behaved with respect to insertions as they usually act with respect to initial conditions. The Shuman scheme requires some adjustment of the initial fields (see, e.g., Haltiner, 1971, p. 269) because of its lack of internal viscosity. The Matsuno-TASU scheme on the other hand requires no balancing of the initial field (see Somerville *et al.*, 1974), in all likelihood because of its strong filtering and damping properties. These schemes behave entirely similarly with respect to data insertion, as described above.

The impact of data insertion on the energy spectra seemed to be contrary to the expected results. Instead

of creating small shocks which give rise to high-wavenumber oscillations, the insertion of computer-produced data transferred high-wavenumber energy created by poor initial conditions to the lower wavenumber region. This may be seen as due to essentially the reinitialization of the entire field with the inserted data, which have already been carefully filtered by the M-A model. If real atmospheric observations were used, this shift in the energy spectra may well have been in the other direction.

In the future, research should center about the use of actual data rather than computer simulations. This should help determine which of the numerical schemes are best equipped to handle expected satellite observations of the real atmosphere and what possible methods can be introduced to improve their assimilation.

Acknowledgments. The author wishes to express his gratitude to Drs. R. Somerville and P. Stone of the Goddard Institute for Space Studies (GISS) for their comments and suggestions. All computations were performed on the IBM 360/95 at GISS. This research was supported in part by NASA Contracts NGR 33-008-191 and NGL 33-016-013.

APPENDIX

Details of the Schemes

a. Shuman scheme

The details of the Shuman scheme are described in Haltiner (1971). Eq. (1) written in terms of this method become

$$\left. \begin{aligned} \bar{u}_i^t &= \overline{f\bar{v}^{xy} - m\bar{u}^{xy}\bar{u}_x^y - \bar{v}^{xy}\bar{u}_y^x} - \bar{m}^{xy}\bar{\phi}_x^y \\ \bar{v}_i^t &= -(\overline{f\bar{u}^{xy} + m\bar{u}^{xy}\bar{v}_x^y + \bar{v}_y^x} + \bar{\phi}_y^x) \\ \bar{\phi}_i^t &= \bar{\phi}^{xy} - \frac{v}{m} \frac{\partial m}{\partial y} - \bar{\phi}^{xy}\bar{v}_y^x - m\bar{\phi}^{xy}\bar{u}_x^y - \bar{v}\bar{\phi}_y^x - m\bar{u}\bar{\phi}_x^y \end{aligned} \right\},$$

where $\bar{A}^x = \frac{1}{2}(A_{j+1} + A_{j-1})$ and $A_x = (1/\Delta x)(A_{j+1} - A_{j-1})$. There are differences between the equations presented here and those given by Haltiner (1971, p. 228) because of the staggered grid system employed in these experiments.

All terms are evaluated in the center of a grid box consisting of four points. The final value for a grid point is determined by averaging the values in the four surrounding box centers. Extensive smoothing is thus accomplished at each time step.

b. Matsuno-TASU scheme

A complete description of this scheme is given by Arakawa (1972). The Matsuno time-differencing method involves a predictor-corrector computation

with two iterations at each time step as described in Section 3. TASU space differencing alternates with centered differencing once every five time steps. The TASU differencing involves taking x -differences centered $\Delta y/2$ above the central point and $\Delta x/2$ to the right for y -differences during one time step, then taking differences below and to the left for the next time step. The TASU differencing is performed only during the second of the Matsuno time steps. The sequence will then look like this for six time steps:

| Time step | Time difference | Space difference |
|-----------|-----------------|------------------|
| 1 | forward | centered |
| | backward | centered |
| 2 | forward | centered |
| | backward | centered |
| 3 | forward | centered |
| | backward | centered |
| 4 | forward | centered |
| | backward | centered |
| 5 | forward | centered |
| | backward | upper-right |
| 6 | forward | centered |
| | backward | lower-left |

c. Semi-implicit scheme

Many implicit and semi-implicit methods have been devised to avoid the restriction on the time step imposed by the Courant-Friedrichs-Lewy condition for linear stability. The one used for this study is based on the scheme devised by McPherson (1971).

The equations of motion are written in difference form with all but the advective terms given at the same time step:

$$\left. \begin{aligned} (u^{n+1} - u^k)/D + m \left(u^n \frac{\partial u^n}{\partial x} + v^n \frac{\partial u^n}{\partial y} \right) + m \frac{\partial \phi^{n+1}}{\partial x} - f v^{n+1} &= 0 \\ (v^{n+1} - v^k)/D + m \left(u^n \frac{\partial v^n}{\partial x} + v^n \frac{\partial v^n}{\partial y} \right) + \frac{\partial \phi^{n+1}}{\partial y} + f u^{n+1} &= 0 \end{aligned} \right\}, \quad (A1)$$

where $D = 2\Delta t$ and $k = n-1$ except when $n=0$. (At $n=0$, $D = \Delta t$ and $k=0$.) Eliminating v^{n+1} from the first equation and u^{n+1} from the second equation leaves explicit equations for u^{n+1} and v^{n+1} in terms of ϕ^{n+1} as follows:

$$\lambda u^{n+1} = B - D \left(m \frac{\partial \phi^{n+1}}{\partial x} + f D \frac{\partial \phi^{n+1}}{\partial y} \right), \quad (A2)$$

$$\lambda v^{n+1} = A - D \left(\frac{\partial \phi^{n+1}}{\partial y} - f D m \frac{\partial \phi^{n+1}}{\partial x} \right), \quad (A3)$$

where

$$\lambda = 1 + f^2 D^2,$$

$$A = v^k - f D u^k + D \left[f D \left(m u^n \frac{\partial u^n}{\partial x} + v^n \frac{\partial u^n}{\partial y} \right) - \left(m u^n \frac{\partial v^n}{\partial x} + v^n \frac{\partial v^n}{\partial y} \right) \right],$$

$$B = u^k + f D v^k - D \left[f D \left(m u^n \frac{\partial v^n}{\partial x} + v^n \frac{\partial v^n}{\partial y} \right) + \left(m u^n \frac{\partial u^n}{\partial x} + v^n \frac{\partial u^n}{\partial y} \right) \right].$$

The continuity equation in finite-difference form yields

$$\phi^{n+1} + D m u^n \frac{\partial \phi^n}{\partial x} + D v^n \frac{\partial \phi^n}{\partial y} + D \phi^n \left(m \frac{\partial u^{n+1}}{\partial x} + \frac{\partial v^{n+1}}{\partial y} \right) - m^{-1} D \phi^n v^n \frac{\partial m}{\partial y} = \phi^K. \quad (\text{A4})$$

Differentiating (A2) with respect to x , (A3) with respect to y (neglecting the latitudinal change of f and m), and adding, yields an expression for the velocity divergence at time $n+1$ in terms of ϕ^{n+1} and known quantities. Substituting for the divergence in (A4) yields

$$\nabla^2 \phi^{n+1} - \lambda \phi^{n+1} (D^2 \phi^n)^{-1} = \lambda F^n (D^2 \phi^n)^{-1}, \quad (\text{A5})$$

where ∇^2 is the Laplacian operator $[(\partial^2/\partial x^2) + (\partial^2/\partial y^2)]$ while

$$F^n = \phi^n D \left(\frac{\partial A}{\partial y} + m \frac{\partial B}{\partial x} \right) + D \left(m u^n \frac{\partial \phi^n}{\partial x} + v^n \frac{\partial \phi^n}{\partial y} \right) - D \phi^n v^n m^{-1} \frac{\partial m}{\partial y} - \phi^k$$

is a known function of space at each time step.

Eq. (A5), given in Section 3, can be solved numerically by means of a relaxation technique. The relaxation was performed sequentially so that lower-left values were immediately replaced by the new values. The remainder R was thus determined at each point j, l by

$$R_{j,l}^m = \phi_{j,l}^{n+1} + m^2 (\Delta y)^2 (\Delta x)^{-2} (\phi_{j+1,l}^m + \phi_{j-1,l}^{n+1}) - \phi_{j,l}^m [2 + 2m^2 (\Delta y)^2 (\Delta x)^{-2} + \lambda (D^2 \phi^n)^{-1}] - \lambda F^n (D^2 \phi^n)^{-1}, \quad (\text{A6})$$

where the superscript in terms of m refers to the iteration number. Once R^m is determined, the value of ϕ^{n+1} is calculated by over-relaxation, i.e., by adding to ϕ^m the quantity $1.5 R^m [2 + 2m^2 (\Delta y)^2 (\Delta x)^{-2} + \lambda (D^2 \phi^n)^{-1}]^{-1}$. Iterations continued until all $R_{j,l} \leq 10^{-3}$. The number of iterations required for this accuracy ranged between 35 and 40 at each time step.

REFERENCES

- Arakawa, A., 1972: Design of the UCLA general circulation model. Tech. Rept. No. 7, Dept. of Meteorology, University of California at Los Angeles.
- Gates, W. L., E. S. Batten, A. B. Kahle and A. B. Nelson, 1971: A documentation of the Mintz-Arakawa two-level atmospheric general circulation model. Rand Corporation, Rept. R-877-ARPA.
- Grammelvedt, Arne, 1969: A survey of finite-difference schemes for the primitive equations for a barotropic fluid. *Mon. Wea. Rev.*, **97**, 384-404.
- Haltiner, G. J., 1971: *Numerical Weather Prediction*. New York, Wiley, 317 pp.
- Hayden, Christopher M., 1973: Experiments in the four-dimensional assimilation of Nimbus SIRS data. *J. Appl. Meteor.*, **12**, 425-436.
- Jastrow, R., and M. Halem, 1973: Simulation studies and the design of the first GARP global experiment. *Bull. Amer. Meteor. Soc.*, **54**, 13-21.
- Kasahara, A., 1972: Simulation experiments for meteorological observing systems for GARP. *Bull. Amer. Meteor. Soc.*, **53**, 252-264.
- McPherson, Ronald D., 1971: Note on the semi-implicit integration of a fine mesh limited area prediction model on an offset grid. *Mon. Wea. Rev.*, **99**, 242-246.
- Somerville, R. C. J., P. H. Stone, M. Halem, J. E. Hansen, J. S. Hogan, L. M. Druyan, G. Russell, A. A. Lacis, W. J. Quirk and J. Tenenbaum, 1974: The GISS model of the global atmosphere. *J. Atmos. Sci.*, **31**, 84-117.